scientific reports

Check for updates

OPEN

Enhanced laser wireless power transmission efficiency with a novel PV-TEG hybrid receiver: dual thermal management and energy recovery

Meng Xian-long[1,2], Wang Zi-kun[1,2], Immanuvel Paul[3,4], Steffy Sara Varghese[5] & Liu Cun-liang[1,2]✉

Laser wireless power transmission (LWPT) has emerged as a transformative solution for medium and long-distance energy delivery, offering a reliable alternative to traditional cable-based systems. However, thermal management and residual energy recovery remain critical challenges at the receiver end, particularly under prolonged high-intensity laser exposure. In this study, a novel hybrid receiver integrating photovoltaic (PV) cells and thermoelectric generators (TEG), termed the PV-TEG system, is proposed and analyzed for the first time in LWPT applications. The PV-TEG system not only enhances energy utilization efficiency but also mitigates the thermal stress on PV cells by converting unused residual heat into supplemental power via the thermoelectric effect. A comprehensive multiphysics simulation model, validated experimentally, was developed to evaluate the thermal, electrical, and optical performance of the PV-TEG system under various laser power levels and atmospheric turbulence intensities. The results reveal that the PV-TEG receiver significantly reduces the operating temperature of PV cells by up to 31.94 K compared to conventional PV-only receivers. This effective thermal management improves the open-circuit voltage and maximum power output of the PV cells, achieving an overall power improvement of 25.81% over standalone PV receivers. Furthermore, under moderate atmospheric turbulence, the PV-TEG system exhibits a notable increase in output power, with enhancements of up to 66.06%. While strong turbulence introduces uneven energy distribution, the PV-TEG receiver maintains superior performance by leveraging its dual energy recovery capability. The study also demonstrates that the photoelectric conversion efficiency of PV cells in the PV-TEG system stabilizes at over 48%, while the thermoelectric conversion efficiency steadily increases with higher laser power. The findings establish the PV-TEG system as a robust and efficient LWPT receiver, capable of addressing key limitations such as thermal degradation and atmospheric energy losses. This pioneering work provides a solid foundation for the practical deployment of PV-TEG receivers in terrestrial, aerospace, and space-based energy applications, marking a significant advancement in the field of wireless power transmission.

The rapid advancements in science and technology, coupled with the increasing prevalence of mobile devices and distributed energy systems, have underscored the inadequacy of traditional contact-based power supply mechanisms in addressing the growing and dynamic energy demands of modern society. As energy requirements diversify across sectors such as portable electronics, electric vehicles, unmanned aerial vehicles (UAVs), and space-based communication networks, the need for innovative, flexible, and high-efficiency energy transmission technologies has become imperative. In this context, Wireless Power Transmission (WPT) has emerged as a transformative solution, offering the capability of delivering point-to-point energy transfer without

[1]School of Power and Energy, Northwestern Polytechnical University, 1 Dongxiang Road, Xi'an 710072, Shaanxi, People's Republic of China. [2]Shaanxi Key Laboratory of Thermal Sciences in Aero-engine System, Northwestern Polytechnical University, Xi'an 710129, Shaanxi, People's Republic of China. [3]Department of Aerospace Engineering, Khalifa University, Abu Dhabi, United Arab Emirates. [4]Center for Membranes and Advanced Water Technology (CMAT), Khalifa University, Abu Dhabi, United Arab Emirates. [5]School of Engineering, Architecture and Interior Design, Amity University Dubai, Dubai, United Arab Emirates. ✉email: liucunliang@nwpu.edu.cn

the constraints and limitations posed by conventional wired systems. WPT holds the potential to revolutionize critical domains including defense, industrial automation, communications, smart grids, and aerospace applications.

The concept of WPT dates back to the groundbreaking work of Nikola Tesla in 1904[1], who envisioned wireless energy transfer through the Earth's atmosphere. Over the decades, WPT technologies have evolved substantially and can now be classified into three primary paradigms: inductive coupling, magnetic field resonance, and radio frequency (RF) radiation[2].

Inductive coupling[3] and magnetic field resonance[4] have demonstrated exceptional efficacy for short-range applications, such as wireless charging of consumer electronics, electric vehicles, and biomedical implants. However, their performance deteriorates significantly over increasing distances due to exponential decay in field strength. In contrast, RF radiation methods, including microwave wireless power transmission (MWPT)[5] and laser wireless power transmission (LWPT)[6], have emerged as viable solutions for medium to long-range energy delivery. Among these, LWPT offers unique advantages such as high energy density, narrow beam divergence, short wavelength, and excellent spatial precision. These attributes position LWPT as a promising solution for applications in space-based solar power stations[7–9], UAV power systems[10], satellite-to-satellite energy transfer, and power delivery in remote or extreme terrestrial environments[11].

Despite its notable advantages, the practical deployment of LWPT systems is not without challenges. The transmission of laser energy over extended distances is significantly impeded by atmospheric effects, which include absorption and scattering by gas molecules and aerosols, beam broadening and fluctuations caused by turbulence, and thermal nonlinearities that distort beam propagation[12]. Atmospheric propagation models, such as Beer's law for absorption and Rayleigh and Mie scattering theories[13], are commonly used to analyze these effects. Predictive tools like MODTRAN and LOWTRAN, though effective, often fail to fully capture the inherent stochastic variability of real-world atmospheric interactions. In recent years, numerical simulations have emerged as an alternative approach, offering higher precision and controllability in modeling beam propagation losses and turbulence[14,15].

At the receiving end, efficient energy conversion remains critical for LWPT systems. When laser energy irradiates PV cells, electrical power is generated via the photoelectric effect. However, a substantial fraction of unabsorbed laser energy manifests as waste heat, which raises the operating temperature of PV cells. This thermal load adversely impacts their performance by reducing the open-circuit voltage and short-circuit current, leading to a decline in photoelectric conversion efficiency. It is well-documented that for every 1°C rise in temperature, the efficiency of conventional PV cells decreases by approximately 0.3–0.5%. This issue is particularly pronounced in continuous, high-intensity laser exposure scenarios.

To address these limitations, the integration of thermoelectric generators (TEGs) with PV systems has emerged as a promising hybrid solution. TEGs operate based on the Seebeck effect, which enables the conversion of temperature gradients into electrical energy[16]. By harnessing the waste heat generated from PV cells, TEGs not only enhance overall energy conversion efficiency but also provide an effective means of thermal management, thereby stabilizing PV cell performance. Recent investigations[17–20] have demonstrated that PV-TEG hybrid systems can extend the operational lifespan of PV cells, reduce thermal stress, and recover residual energy as supplementary power[21].

For LWPT receivers, the integration of PV cells with TEG modules represents a paradigm shift, offering a transformative approach to overcoming the challenges posed by thermal degradation and atmospheric energy losses. To the best of the authors' knowledge the PV-TEG system was never tested for the LWPT in the literature. The PV-TEG system ensures the optimal utilization of laser energy by combining optical, thermal, and electrical processes. The unconverted laser energy is absorbed as thermal energy in the TEG module, which subsequently generates additional electrical power. Simultaneously, the temperature rise in PV cells is mitigated, preserving their operational efficiency under continuous laser irradiation. This dual functionality makes PV-TEG systems particularly suitable for LWPT receivers operating in high-intensity, real-world conditions.

In this study, a comprehensive multiphysics model has been developed to analyze the performance of PV-TEG systems under realistic environmental conditions. The model accounts for atmospheric attenuation, turbulence effects, and laser beam characteristics during medium and long-range energy transmission. The optical field distribution of the laser beam is simulated, and the thermal and electrical performance of the PV-TEG system is evaluated under varying operational scenarios. A comparative analysis of PV-TEG systems with standalone PV receivers is presented to highlight the substantial improvements achieved in energy conversion efficiency and thermal management.

The novel contributions of this work include:

1. Development of a robust multiphysics simulation model to analyze the interplay between optical, thermal, and electrical phenomena in PV-TEG systems.
2. Evaluation of the impact of atmospheric turbulence, beam attenuation, and propagation losses on the performance of LWPT systems.
3. Demonstration of significant enhancements in energy conversion efficiency, thermal management, and output stability achieved by PV-TEG hybrid systems compared to standalone PV receivers.

The results presented in this study provide valuable insights into the optimization of LWPT receivers for terrestrial and aerospace applications. By addressing critical challenges related to atmospheric disturbances, energy losses, and thermal effects, this work lays a strong foundation for the practical deployment of PV-TEG systems in next-generation wireless power transmission technologies. The proposed approach paves the way for reliable and sustainable energy delivery in diverse and challenging operational environments.

Mathematical models

In this section, a simulation model of the TEG module is developed based on the fundamental principles of the thermoelectric effect. The TEG module integrates P-type and N-type bismuth telluride particles, connected in series, to achieve a higher output voltage and enhanced power generation. The thermal energy driving the TEG module is derived from two primary sources: the operational temperature of the PV cell and the unabsorbed portion of the laser beam energy that is not directly utilized by the PV cell for electrical conversion. This design ensures efficient harnessing of the residual thermal energy, thereby contributing to the overall improvement in energy utilization efficiency.

Simulation model of TEG module

The temperature of the TEG system is governed by the following unsteady conduction equation:

$$\rho c\frac{\partial T}{\partial t}+\nabla\cdot\vec{q}=\Phi \tag{1}$$

where ρ is the density of the material, T is the temperature, t is time, $\bar{q}$ is the heat flux density, and Φ is the heat generated by the heat source per unit volume per unit time. The boundary conditions of this formula are: $Q_{\mathrm{bottom}}=0$, $Q_{\mathrm{top}}=Q_s$. This equation is used along with the following charge continuity equation to mathematically model the TEG.

In a single electric field, the charge continuity equation is:

$$\nabla\cdot\left(\vec{J}+\frac{\partial\vec{D}}{\partial t}\right)=\nabla\cdot\vec{J}+\frac{\partial}{\partial t}\left(\nabla\cdot\vec{D}\right)=0 \tag{2}$$

where $\bar{J}$ is the amount of free charge flowing out per unit volume per unit time (i.e., current density), $\frac{\partial\vec{D}}{\partial t}$ is the increment of free charge per unit volume per unit time, and $\vec{D}$ is the electric flux density.

The relationship between electric flux density $(\vec{D})$ and the electric field $(\vec{E})$ is expressed as:

$$\vec{D}=\epsilon\vec{E} \tag{3}$$

where ϵ is the permittivity of the material.

At the same time, the electric field $(\vec{E})$ is related to the electric potential (ϕ) as:

$$\vec{E}=-\nabla\phi \tag{4}$$

Therefore, the electric flux density is related to the electric potential as,

$$\vec{D}=-\epsilon\nabla\phi \tag{5}$$

The flow of current in TEG is not only due to electric potential but also due to the temperature gradient. Therefore, the current density is written as,

$$\vec{J}=-\sigma\nabla\phi-\sigma[\alpha]\nabla T \tag{6}$$

where σ is the electric conductivity of the material, and α is the Seebeck coefficient.

The heat flux for the TGE is given as,

$$\vec{q}=-k\nabla T+[\alpha]T\bar{J} \tag{7}$$

Finally, the internal heat generation (Φ) is given as,

$$\Phi=\vec{J}\cdot\vec{E} \tag{8}$$

Substituting Eqs. (6) and (4) into the above equation the internal heat generation becomes,

$$\Phi=\sigma|\nabla\phi|^2+\sigma[\alpha](\nabla T\cdot\nabla\phi) \tag{9}$$

After collation of the aforementioned equations, a system of differential equations for thermoelectric coupling is obtained:

$$\rho c\frac{\partial T}{\partial t}+\nabla\cdot\left[-k\nabla T+[\alpha]T\left(-\sigma\nabla\phi-\sigma[\alpha]\nabla T\right)\right]=\sigma|\nabla\phi|^2+\sigma[\alpha](\nabla T\cdot\nabla\phi) \tag{10}$$

$$\epsilon\frac{\partial}{\partial t}\left[\nabla\cdot\nabla\phi\right]+\nabla\cdot\left(\sigma\nabla\phi\right)+\nabla\cdot\left(\sigma[\alpha]\nabla T\right)=0 \tag{11}$$

The solution of the thermoelectric coupling process involves solving the above two coupled equations for temperature and electric potential. To this end, we use COMSOL software.

	Material	Length (mm)	Width (mm)	Height (mm)	Quantity (1)
Cold and hot end faces	Alumina	40	40	1	2
Thermoelectric particles	Bi_2Te_3	1.4	1.4	1.7	254
Conductive copper sheet	Copper	3.8	1.7	0.1	255

Table 1. Geometric parameters of the TEG.

	Constant pressure heat capacity (J/(kg K))	Density (kg/m^3)	Thermal conductivity (W/(m K))	Electrical conductivity (S/m)	Seebeck coefficient (V/K)
Alumina	900	3900	27	–	–
Copper	385	8960	400	$5.998e^7$	–
Bi_2Te_3	154	7700	$k(T)$	$\sigma(T)$	$1.90e^{-4}$

Table 2. Physical parameters of Bi_2Te_3.

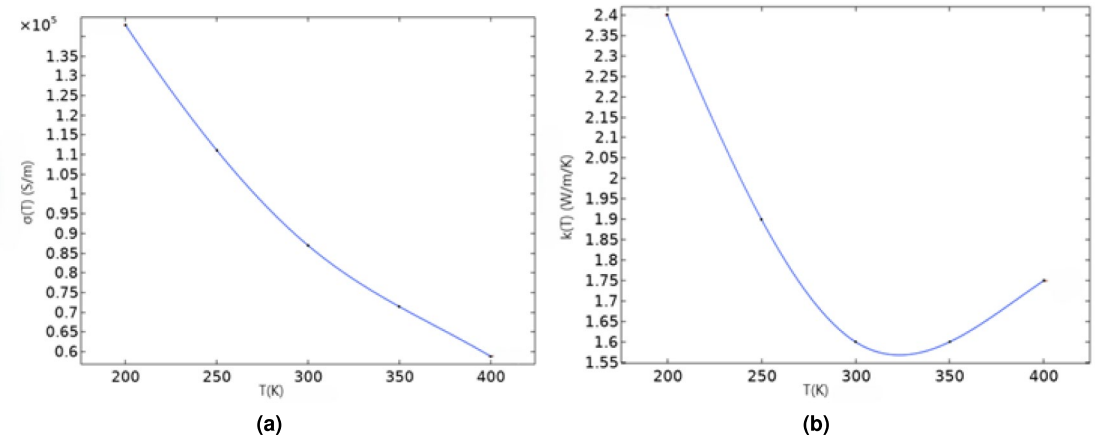

Fig. 1. Variation of (**a**) thermal conductivity and (**b**) electrical conductivity with respect to temperature.

The TEG module typically consists of alumina ceramic plates that serve as the cold and hot ends, thermoelectric materials, and copper sheets for electrical connections. By connecting multiple thermoelectric unit modules in series, a complete TEG module is constructed.

In this study, alumina ceramic substrate is used for the cold and hot ends of the temperature difference power generation module, which has good conductivity, mechanical strength, and high-temperature resistance. The conductive copper sheets are arranged on the alumina ceramic substrate at equal intervals, and the P-type and N-type Bi_2Te_3 (bismuth telluride) particles are connected in series through the conductive copper sheets. In practice, the number of thermoelectric unit pairs in the TEG module is usually determined according to the performance requirements, and the 127 pairs of thermoelectric units commonly used in commercial TEG modules are used as the research object. Table 1 lists the geometric parameters of each component of the differential power generation module.

Bi_2Te_3 is used as the thermoelectric material for TEG in this model, but no distinction is made between P-type materials and N-type materials in the multiphysics simulation software. According to the Seebeck effect, the temperature electromotive force of P-type semiconductors is directed from the high-temperature side to the low-temperature side (Seebeck coefficient is positive), while that of N-type semiconductors is the opposite, so the Seebeck coefficient of P-type bismuth telluride particles is set to S and $-S$ for N-type bismuth telluride particles when setting the material properties. Table 2 shows the physical parameters required for the materials used in each component of the TEG module. The thermal conductivity $k(T)$ and electrical conductivity $\sigma(T)$ are expressed as a function of temperature, as shown in Fig. 1, and the image data is from the COMSOL Materials Database.

Thermal conductivity decreases significantly with rising temperature, reaching a minimum around 300–350 K. This behavior arises due to increased phonon-phonon scattering at higher temperatures, which reduces the ability of the material to conduct heat. Electrical conductivity decreases monotonically with temperature, indicating a reduction in carrier mobility caused by enhanced phonon scattering as temperature rises. The material retains good conductivity across the range, crucial for efficient thermoelectric performance. The combined trends highlight a balance between heat conduction and charge transport, making the material suitable for thermoelectric applications, particularly in the PV-TEG hybrid system for energy recovery.

In the multiphysics simulation, the TEG module primarily employs the electric current module, the solid heat transfer module, and the thermoelectric effect module. These modules are utilized to define the current distribution within the thermoelectric units and the thermal conductive copper sheets, as well as to describe the solid heat transfer throughout the entire TEG module.

Within the thermoelectric module, two vacant conductive copper sheets are included: one is grounded, while the other is used to detect the electric potential. To simulate realistic thermal conditions, convective heat transfer boundary conditions are applied at the cold end of the module, while a constant temperature boundary condition is imposed at the hot end. This configuration ensures an accurate representation of the heat flow and electric potential distribution within the TEG module.

PV-TEG simulation & laser transmission simulation model

To enhance the energy utilization efficiency of the receiver, a hybrid PV-TEG receiver has been developed, comprising GaAs PV cells and a TEG module. This design not only reduces the operational temperature of the PV cells under continuous laser irradiation, thereby prolonging their service life and maintaining good output performance, but also utilizes the waste heat generated by the PV cells to produce additional thermoelectric power. This dual mechanism significantly improves the overall energy utilization efficiency.

A laser wireless power transmission (LWPT) system typically consists of two main components: the laser transmitter and the laser receiver. When aberration and thermal effects are negligible, the laser emitted from a circular aperture-stabilized cavity follows a Gaussian beam profile. The intensity distribution of a Gaussian beam in a vacuum is circularly symmetric across any plane perpendicular to the optical axis and can be expressed as[22]:

$$u_0(x,y,z) = c \cdot e^{-\frac{r^2}{\omega^2(z)}} e^{-i\left[kz+\arctan\left(\frac{z}{R}\right)\right]}, \tag{12}$$

where c is the amplitude constant, λ is the laser wavelength, k is the wave number, and $\omega(z)$ is the beam waist radius.

In simulating the output characteristics of PV cells, a single-diode circuit model is employed. The simulation involves finite element analysis (FEA) to incorporate the laser's light field distribution as a surface variable on the PV cells. The thermoelectric coupling characteristics of the PV cells are modeled to predict their output characteristics accurately. During the modeling process, the illuminated and dark regions of the PV cells are defined separately. The current generated per unit thickness in the illuminated (Q_e) and dark (Q_d) regions is expressed as:

$$Q_e = C_1 G + C_2 T^3 \exp\left(-\frac{T_1}{T}\right)\left[\exp\left(\frac{V_j}{nV_T}\right) - 1\right] + C_3 V_j, \tag{13}$$

$$Q_d = C_2 T^3 \exp\left(-\frac{T_1}{T}\right)\left[\exp\left(\frac{V_j}{nV_T}\right) - 1\right] + C_3 V_j, \tag{14}$$

The fitting parameters in these formulae are shown in Table 3.

The effect of atmospheric turbulence on laser transmission is also analyzed. Turbulence causes random fluctuations in the wavefront phase of the transmitted beam due to variations in atmospheric density caused by changes in temperature and pressure. These random refractive index fluctuations lead to intensity flickering, beam jitter, and spot expansion. Numerical simulations, including the turbulence phase screen method, are commonly used to model these effects, as shown in Fig. 2a.

The Kolmogorov turbulence power spectrum model describes the power spectral density as[23]:

$$\Phi_{\kappa_z}(\kappa_z) = 0.033 C_n^2(\zeta)\kappa^{-11/3}, \tag{15}$$

where ζ is the propagation direction and $C_n^2(\zeta)$ represents the turbulence intensity structure constant. The corresponding atmospheric phase power spectrum for a thin layer is:

$$F_\phi(\kappa_x,\kappa_y) = 0.066\pi k^2 C_n^2 \Delta\zeta(\kappa_x^2+\kappa_y^2)^{-11/3}. \tag{16}$$

Figure 2b illustrates the PV-TEG receiver's structure. The PV-TEG receiver consists of GaAs photovoltaic cells and a TEG module. The photovoltaic cells are positioned at the geometric center of the thermoelectric module's hot end and are bonded using thermally conductive adhesive. The adhesive's thermal conductivity is $k = 2.0\ \mathrm{W/(m \cdot K)}$, with a density $\rho = 2500\ \mathrm{kg/m^3}$ and specific heat capacity $C_p = 1046\ \mathrm{J/(kg \cdot K)}$. The heat sink of photovoltaic cells is small in quality, the heat capacity is small, the battery material is very thin, and the semiconductor material has good thermal conductivity, which is easy to dissipate heat and achieve steady state. At the same time, although the thermal conductivity of the thermal conductivity adhesive itself is not high, it ensures close thermal contact between the photovoltaic cell and the TEG module, avoiding local hot spots

Material	C_1, A/W	$C_2, A/m^2K^3$	$C_3, A/m^2V$
GaAs	2.63e-5	-8477.41	-9.98e-4

Table 3. Fitting parameters.

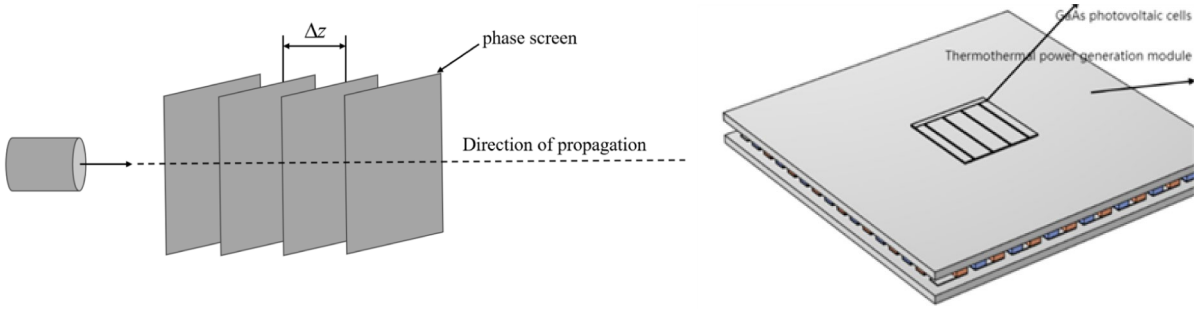

Fig. 2. (**a**) Schematic diagram of the turbulent phase screen method, (**b**) schematic diagram of the PV-TEG receiver.

	Material	Density (kg/m^3)	Thermal Conductivity (W/(m K))	Constant Pressure Heat Capacity (J/(kg K))
Main grid line	Copper	8960	400	385
Secondary grid line	Copper	8960	400	385
GaAs Substrate	GaAs	5320	55	320

Table 4. Thermal characterization parameters of PV cell components.

caused by poor contact, so as to evenly distribute the heat. These parameters ensure efficient thermal coupling between the PV cells and the thermoelectric module.

Heat transfer characteristics and meshing

In a laser wireless energy transmission system, the operational temperature of the PV cell at the receiving end significantly impacts its output performance. Therefore, it is crucial to analyze the heat transfer characteristics of the PV cell. In modeling the heat transfer processes in PV cells, the primary heat source is attributed to the portion of laser energy not converted into electrical energy. The heat transfer mechanisms include the internally generated heat within the PV cell and the conductive heat exchange between the various components of the PV cell.

To account for the external laser heat source and the internal heat source at the receiving end, the receiver system is modeled holistically. The difference between the total laser energy absorbed at the receiving end and the energy converted into electrical power represents the heat source within the receiver system. The boundary heat source Q, generated on the surface of the PV cell, is defined in the simulation model as follows:

$$Q = G \times (1 - \eta_{\text{electric}}), \tag{17}$$

where G denotes the distribution of laser power received on the surface of the PV cell, and η_{electric} represents the ratio of the output power of the PV cell to the received energy. The heat transfer characteristics of each component within the PV cell are summarized in Table 4.

The interaction between the outer surface of the receiving terminal and the external environment is modeled using convective heat transfer boundary conditions. The external ambient temperature is set to $293.15\ \text{K}$ in the simulation. Laser energy is the dominant energy source at the receiving end, and the surface of the PV cell interacts with the laser according to the heat source defined in Eq. (17). The outer surface of the PV cell is in thermal contact with the environment, with a convective heat transfer coefficient of $16\ \text{W}/(\text{m}^2 \cdot \text{K})$ to represent heat transfer with the external environment.

To enhance computational efficiency, an unstructured mesh is employed for the model. The meshing effect for each component of the PV-TEG receiving end is illustrated in Fig. 3. The mesh density is refined in regions of significant heat transfer, such as the contact position between the PV cell and the hot end of the TEG module, while coarser meshing is applied to the thermoelectric module. The average grid mass for the overall mesh is 0.6256, and for the GaAs PV cell, it is 0.9236, ensuring that the meshing meets the accuracy requirements. The average irradiation intensities for PV-TEG and PV receivers (Table 9) are calculated by integrating the Gaussian beam profile (Eq. 12) over their respective areas. The PV-TEG receiver's larger area (40×40 mm in Table 1) results in a lower average intensity (3242.5 W/m^2) compared to the PV receiver (8849.2 W/m^2), reflecting the beam's spatial energy distribution.

To confirm the grid independence of the simulation results, meshes of varying resolutions were tested under a laser irradiation intensity of $6\ \text{W}$ at a distance of $1\ \text{m}$ from the receiver. A comparison between the existing results and those obtained using an encrypted grid reveals no significant changes in the temperature distribution at the receiving end, thereby validating the reliability of the chosen mesh configuration.

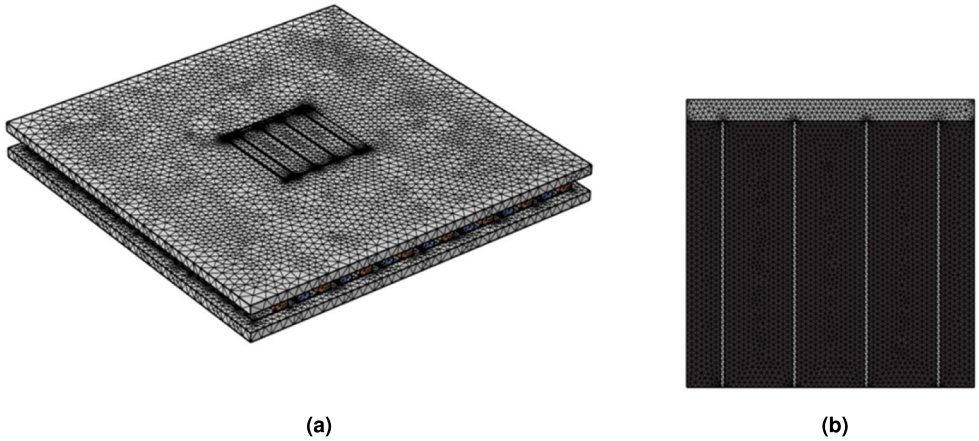

Fig. 3. Computational mesh of: (**a**) PV-TEG receiver, (**b**) photovoltaic cell.

The experimental verification of the PV and TEG systems

In order to explore the output characteristics of the combined thermoelectric system as the receiving end of the laser wireless energy transmission system, this section first takes the TEG module as the research object, simulates the output performance of the TEG module under different boundary conditions through multiphysics simulation, and builds an experimental test platform to test the module to verify the accuracy of the multiphysics simulation model.

In this study, a multiphysics model of the TEG module was developed and validated against experimental results using the commercial thermoelectric module SP1848-27145. The experimental setup of PV is shown in Fig. 4a. The experimental setup was designed to evaluate the output performance of the PV. Figure 4b shows the experimental and fitting I-V curve data of GaAs photovoltaic cells under different irradiation intensities. Figure 4c shows the output performance of this type of temperature difference power generation module through the construction of an experimental test platform to test the output performance of this type of temperature difference power generation module.The comparison between the experimental results and the simulation results is shown in Fig. 4d. The experimental results show that when the temperature of the hot end is 30–80 $^{\circ}$ C, the experimental TEG open circuit voltage is slightly lower than the simulation results. In the experimental process, the hot end of the thermostatic heating table of the thermostatic power generation module is in contact to ensure that the temperature of the hot end meets the constant temperature conditions, but the convective heat transfer coefficient between the cold end and the external environment cannot be completely consistent with the simulation, so the experimental data and the simulation results are deviated. At the same time, with the increase of the temperature of the hot end, the gap between the experimental data and the simulation results is getting smaller and smaller, because in the real environment, the Seebeck coefficient of thermoelectric materials usually increases with the increase of temperature, and under the same temperature difference, the increase of the Seebeck coefficient will lead to the increase of the open-circuit voltage of the thermoelectric power generation module, but in the multiphysics simulation, the Seebeck coefficient is a certain value, so the above phenomenon occurs, but from the overall data comparison, the experimental measured data are basically consistent with the simulation results. Therefore, the accuracy of the multiphysics model is demonstrated.At the same time, the reason why the Seebeck coefficient is determined is studied experimentally, and the conclusions are as follows:

Figure 5a, b show the changes in potential (mV) and temperature (K) of the PV-TEG module when the Seebeck coefficient is set as shown in the article. Figure 5c, d show the potential (mV) and temperature changes of the Seebeck coefficient as it changes with temperature. From Fig. 5a, c, it can be seen that the change in Seebeck's coefficient has little effect on the potential difference between the two ends of PV-TEG, and from Fig. 5b, d, it can be seen that the change in Seebeck's coefficient has little effect on the surface temperature of PV-TEG. Therefore, in order to optimize the calculation and experimental influence, a fixed Seebeck coefficient was selected.

Moreover, it is well-established that the Seebeck coefficient of thermoelectric materials increases slightly with temperature under real operating conditions. This temperature dependence enhances the open-circuit voltage at higher temperature differences. However, the multiphysics simulation assumes a constant Seebeck coefficient, which simplifies the model but introduces slight deviations at lower temperatures. As the hot-end temperature increases, this gap between the experimental and simulated values narrows, indicating that the temperature-dependent behavior of the Seebeck coefficient contributes significantly to the observed experimental trends.

Despite these minor deviations, the overall agreement between the experimental data and the simulation results validates the accuracy and reliability of the developed multiphysics model. The close correlation demonstrates the model's capability to predict the thermal and electrical behavior of TEG modules under realistic conditions. This validation provides confidence in utilizing the model for further optimization and integration of thermoelectric modules in hybrid PV-TEG systems for enhanced energy recovery.

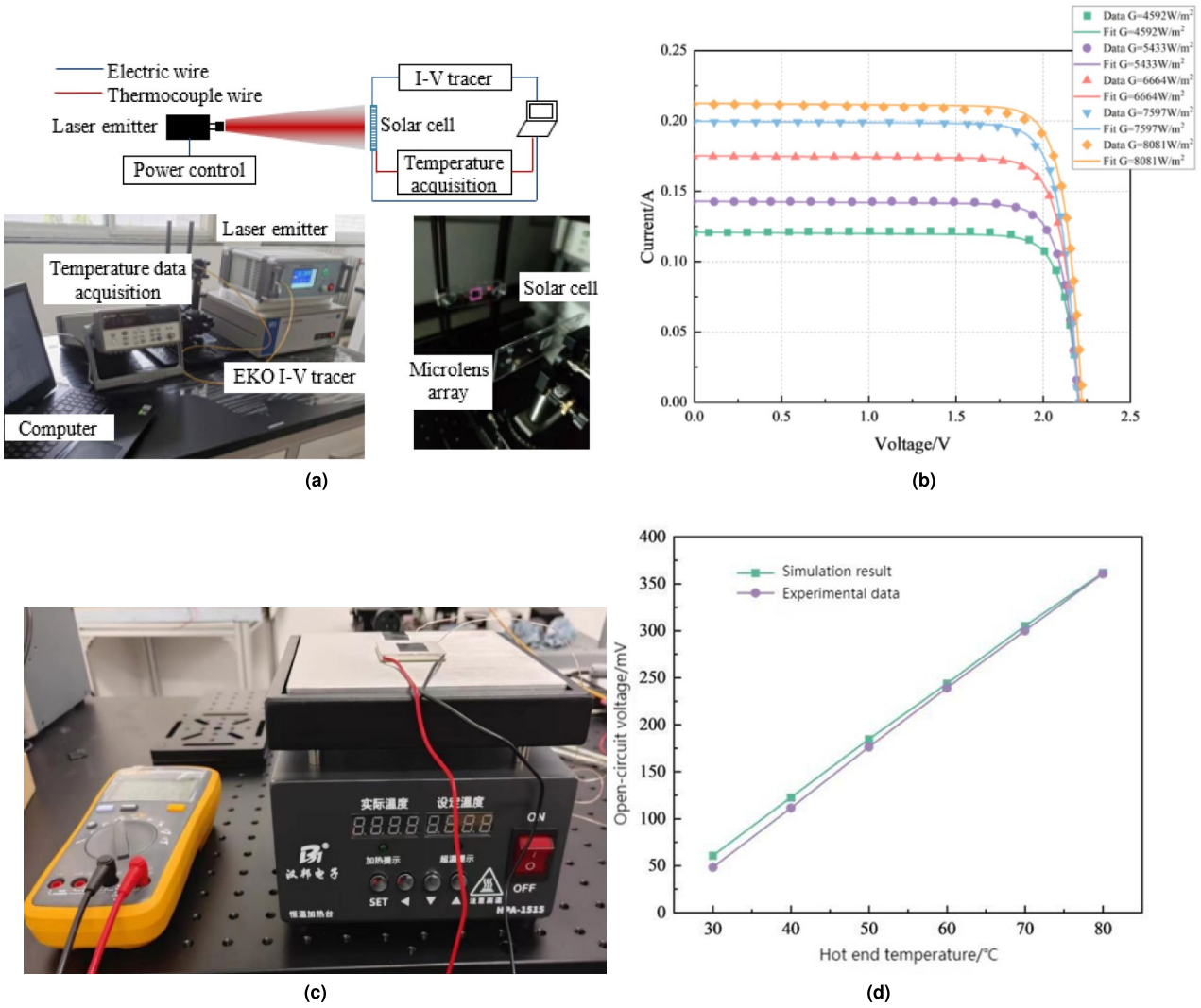

Fig. 4. (**a**) Typical experimental setup, (**b**) I–V characteristic curve of GaAs photovoltaic cells, (**c**) experimental test of temperature difference power generation module, (**d**) comparison of simulation results and product parameters at different temperature differences.

Results and discussion

Because of the influence of the atmosphere, the light field distribution in the laser wireless energy transmission system at medium and long distances is uneven and random before reaching the receiving end, which reduces the amount of laser energy utilized. To address this issue, a combination of temperature difference power generation and photovoltaic power generating technologies is used to investigate the output characteristics of the PV-TEG receiver.

Evaluation of energy efficiency improvement at the receiving end of PV-TEG hybrid application

The PV-TEG receiver can play a cooling role in the photovoltaic cell while recovering the laser energy that is not irradiated to the surface of the photovoltaic cell and is not converted into electrical energy, and the working temperature of the photovoltaic cell will affect its output performance. In order to evaluate the energy efficiency improvement of the PV-TEG system as the receiver, the PV receiver and PV-TEG receiver were simulated under the same laser light source parameter settings, and the specific parameters of the laser light source are shown in Table 5.

Figure 6 illustrates the surface temperature distribution of photovoltaic cells at two different receivers under identical laser irradiation conditions. The temperature profile in both cases exhibits a trend that is highest at the center and gradually decreases towards the periphery, which is consistent with the Gaussian nature of the incident laser beam.

In the case of the standalone PV receiver, the photovoltaic cell relies solely on natural heat exchange with the surrounding environment. As a result, the surface temperature is considerably high, with an average temperature of approximately 345.82 K. The absence of an additional thermal management mechanism allows the thermal

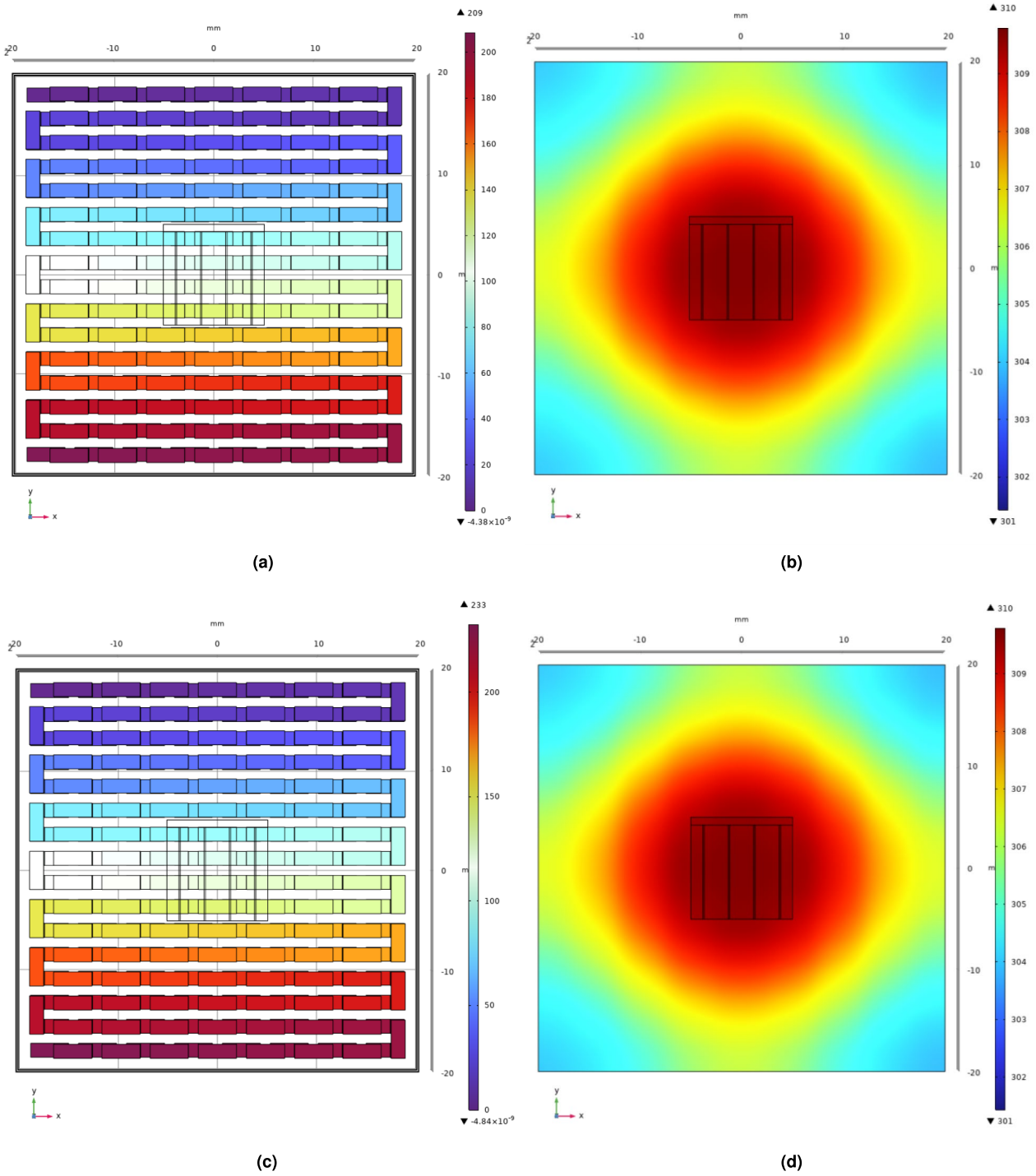

Fig. 5. (**a**) Potential variation of PV-TEG module with constant Seebeck coefficient, (**b**) temperature variation of PV-TEG Module with constant Seebeck coefficient, (**c**) potential variation of PV-TEG module when Seebeck coefficient varies, (**d**) PV-TEG module temperature variation with Seebeck coefficient variation.

Wavelength (nm)	Power (W)	Beam divergence angle (mrad)	Distance (m)	Pattern
808	6	20	1	Continuous

Table 5. Parameters of laser light source.

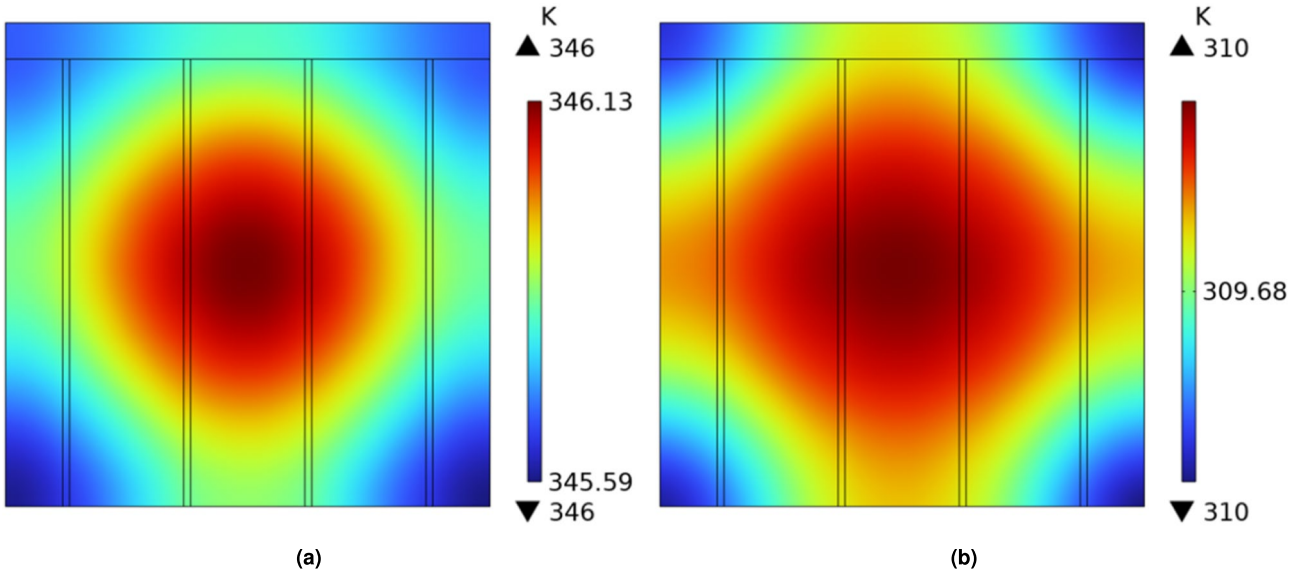

Fig. 6. Surface temperature distribution of photovoltaic cells at two different receivers: (**a**) PV, (**b**) PV-TEG.

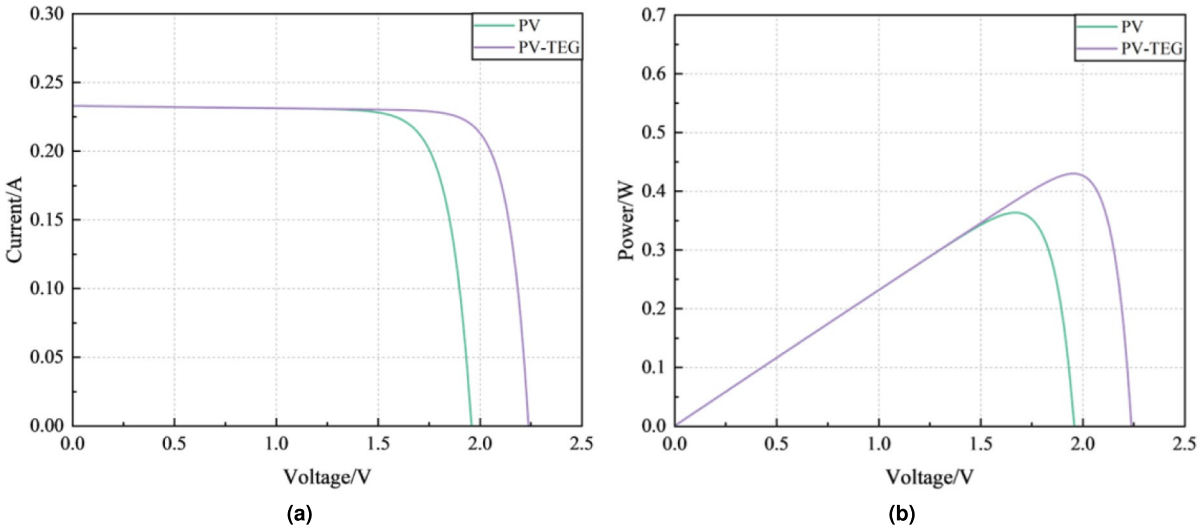

Fig. 7. Comparison of I–V and P–V curves of two different receivers: (**a**) I–V characteristic curves, (**b**) P–V characteristic curves.

energy to accumulate at the center, leading to a pronounced hotspot. In contrast, the PV-TEG receiver, which integrates a TEG with the PV cell, exhibits a significantly lower surface temperature. This reduction is primarily due to the contact between the PV cell and the hot end of the TEG module via a thermally conductive adhesive, which facilitates efficient heat absorption and conversion into electrical energy. The average surface temperature of the PV-TEG receiver is approximately 309.88 K, which represents a temperature reduction of 35.94 K compared to the standalone PV receiver. The results underscore the effectiveness of the PV-TEG system in mitigating thermal buildup. By maintaining a lower operating temperature, the PV-TEG system not only stabilizes the photovoltaic cell's performance but also enhances its operational lifespan and efficiency, particularly under continuous laser irradiation.

In order to evaluate the performance enhancement achieved by the PV-TEG receiver, the output characteristic curves of the two receivers were compared, as illustrated in Fig. 7. The results demonstrate a significant improvement in the open-circuit voltage and maximum power output of the PV cells integrated with the TEG module. This enhancement can be attributed to the effective cooling provided by the TEG module, which reduces the operating temperature of the PV cell, thereby mitigating thermal losses and stabilizing its efficiency. Specifically, the open-circuit voltage of the PV receiver is observed to be 1.96 V, with a corresponding maximum power output of 0.363 W. In contrast, the open-circuit voltage of the PV-TEG receiver increases to 2.24 V, and its maximum power output reaches 0.429 W. This corresponds to an increase of approximately

Receiving end	Subassembly	Open-circuit voltage (mV)	Short-circuit current (mA)	Output power (mW)	Fill factor	Photoelectric conversion efficiency (%)
PV	GaAs battery	1960	232.91	363.32	0.795	41.05%
PV-TEG	GaAs battery	2240	232.91	429.82	0.824	48.57%

Table 6. Output characteristics of PV and PV-TEG receivers.

Open-circuit voltage (mV)	Internal resistance (Ω)	Output power (mW)	Thermoelectric conversion efficiency (%)
233.60	2	27.28	0.58%

Table 7. Output characteristics of the TEG module.

Atmospheric turbulence structure constant ($m^{-2/3}$)	The operating temperature of the PV cell at the receiving end (K)	The operating temperature of the PV-TEG receiver photovoltaic cell (K)
2×10^{-15}	344.90	328.25
2×10^{-14}	312.76	308.22
2×10^{-13}	307.51	310.99

Table 8. Operating temperature of GaAs PV cells at different receivers.

18.1% in the maximum power output compared to the standalone PV receiver. While the short-circuit current remains relatively unchanged between the two configurations, the improved voltage and maximum power output highlight the effectiveness of the PV-TEG system in enhancing energy conversion efficiency through better thermal management. The results underscore the potential of hybrid PV-TEG systems to overcome the limitations of standalone PV receivers under continuous laser irradiation conditions.

In addition, because the laser energy that is not converted into electrical energy gradually increases the surface temperature of the hot end of the TEG module, the temperature difference between the cold and hot ends causes it to generate additional thermoelectric electromotive force, which improves the energy utilization efficiency of the PV-TEG receiver. Table 6 compares the overall output performance of the PV receiver and the PV-TEG joint receiver, and the output characteristics of the TEG module are shown in Table 7.

According to the output characteristics of the photovoltaic cells at two different receivers, it can be seen that under the same laser irradiation, the PV-TEG combined receiver photovoltaic cells show good output performance due to the low working temperature. By combining the GaAs cell with the electrothermal power generation module, the output performance is improved, the operating temperature is reduced, the output power is increased by 66.5mW, the fill factor is increased from 0.795 to 0.824, and the photoelectric conversion efficiency is increased from 41.05% to 48.57%. At the same time, the TEG module obtains a thermoelectric electromotive force of 233.60mV and outputs 27.28mW of power, but the thermoelectric conversion efficiency is only 0.58% because after the receiving end reaches the thermal equilibrium, the temperature difference between the cold and hot ends of the TEG module is small, about 8.3K, and the thermoelectric conversion efficiency can be improved by increasing the temperature difference between the cold and hot ends in the TEG module. The core value of the TEG module lies in energy recovery, and its thermal management effect is a natural consequence of the energy recovery process. Despite the low direct conversion efficiency, it significantly improves the overall performance of the system by recovering waste heat and indirectly improving PV efficiency. In LWPT applications, the energy recovery function of the TEG is the main driver of the system design, and thermal management is an integral additional advantage. The combination of the two makes the PV-TEG system far more energy efficient and reliable than the stand-alone PV system.

In summary, when the total power of the laser beam is 6W, the output power of the receiver is 363.32mW when only PV is used as the receiver, and the total external output power is 457.1mW when the PV-TEG joint receiver is used, and the output performance is improved by 25.81%. The TEG module is designed for energy recovery and active thermal management energy recovery, not as a thermal storage component. As shown in Table 6, the TEG reduces the PV cell temperature by 31.94 K under 6 W laser power, which directly improves PV efficiency from 41.05% to 48.57%. This temperature reduction is achieved by converting residual heat into electrical energy (27.28 mW in Table 7), rather than storing it. The steady-state temperature data in Table 8 further confirm that the TEG prioritizes heat dissipation over thermal retention.There is also some consideration in choosing a laser power of 6W here. Since the maximum power of the laser can be selected as 10W, the laser of 10W will damage the battery to a certain extent, and it is also for the sake of experimental safety. When the laser power is within 6 W, the system behavior is linear or quasi-linear, which facilitates the establishment of theoretical models. The nonlinear effects introduced by higher power can complicate the analysis.

The influence of atmospheric transmission

In order to investigate the enhancement in the performance of the laser wireless energy transmission receiver through the PV-TEG hybrid application over medium and long distances, a comprehensive multiphysics simulation was conducted. Figure 8 illustrates the laser irradiation intensity distribution on the surface of the PV-TEG receiver under varying atmospheric turbulent refractive index structure constants. It is observed that when the atmospheric turbulence intensity, represented by the refractive index structure constants, is relatively low, the PV-TEG receiver demonstrates a significant cooling effect on the operating temperature of the photovoltaic cell. Specifically, the operating temperature of the photovoltaic cell decreases by $16.65\,\mathrm{K}$ and $4.54\,\mathrm{K}$ under moderate turbulence conditions. The magnitude of the temperature reduction is closely related to the non-uniform laser irradiation intensity received on the surface of the photovoltaic cell. However, under conditions of strong atmospheric turbulence, the operating temperature of the photovoltaic cell at the PV-TEG receiver is observed to be higher compared to the standalone PV receiver. This anomaly arises due to the distortion in the spatial distribution of the laser beam caused by atmospheric propagation effects. Consequently, a larger fraction of the laser energy is incident on the hot end of the TEG module rather than on the photovoltaic cell. This uneven energy distribution results in the hot end of the TEG module attaining a higher temperature than the photovoltaic cell. The ensuing reverse heat transfer from the TEG module to the photovoltaic cell causes the cell's temperature to rise by approximately $3.48\,\mathrm{K}$.

These findings highlight the dual influence of atmospheric turbulence on the PV-TEG receiver. While moderate turbulence conditions facilitate efficient cooling and improved thermal management of the photovoltaic cell, strong turbulence leads to beam distortion and localized heating effects, thereby reducing the overall cooling efficiency and increasing the operating temperature of the photovoltaic cell.

In addition to effectively utilizing thermal energy, the TEG module also provides a cooling effect for the PV cells. To demonstrate the optimization of the operating temperature of GaAs photovoltaic cells achieved by the PV-TEG receiver, a comparison of the operating temperatures of the PV cells at the receiving ends of PV-only and PV-TEG systems under varying atmospheric turbulence structure constants is presented in Table 8. The results clearly indicate that the PV-TEG receiver maintains a lower operating temperature for the GaAs photovoltaic cells compared to the PV-only system under low and moderate turbulence conditions. This reduction in temperature enhances the performance and longevity of the photovoltaic cells. However, under strong turbulence, the cooling effect of the PV-TEG system diminishes slightly due to the uneven distribution of laser energy caused by atmospheric distortion.

Figure 9 presents the comparison of output characteristic curves of GaAs PV cells at the receiving ends of the standalone PV receiver and the PV-TEG hybrid receiver under varying atmospheric turbulent refractive index structure constants (C_n^2). When the atmospheric turbulence intensity is low ($C_n^2 = 2 \times 10^{-15}\,\mathrm{m}^{-2/3}$) and moderate ($C_n^2 = 2 \times 10^{-14}\,\mathrm{m}^{-2/3}$), the PV-TEG receiver demonstrates superior performance compared to the standalone PV receiver. Specifically, the open-circuit voltage and maximum power output of the GaAs PV cells at the PV-TEG receiving end show a notable improvement. At $C_n^2 = 2 \times 10^{-15}\,\mathrm{m}^{-2/3}$, the performance enhancement is particularly significant, with the maximum power increasing by 33.76 mW. This improvement is primarily attributed to the thermal management provided by the TEG module, which mitigates the temperature rise in the PV cells and enhances their photoelectric conversion efficiency. However, as the turbulence intensity increases further ($C_n^2 = 2 \times 10^{-13}\,\mathrm{m}^{-2/3}$), the output performance of the PV-TEG receiver deteriorates relative to the standalone PV receiver. This degradation arises due to the non-uniform distribution of laser irradiation intensity caused by severe atmospheric turbulence. Under such conditions, a greater fraction of the laser energy is converted into heat on the surface of the PV-TEG receiver, particularly at the hot end of the TEG module. This localized heating effect increases the operating temperature of the GaAs PV cells, thereby reducing their efficiency and nullifying the thermal benefits of the TEG module. The results underscore that while the PV-TEG hybrid receiver effectively enhances energy conversion performance under low to moderate turbulence intensities, its advantage diminishes under severe turbulence due to uneven irradiation and increased thermal load.

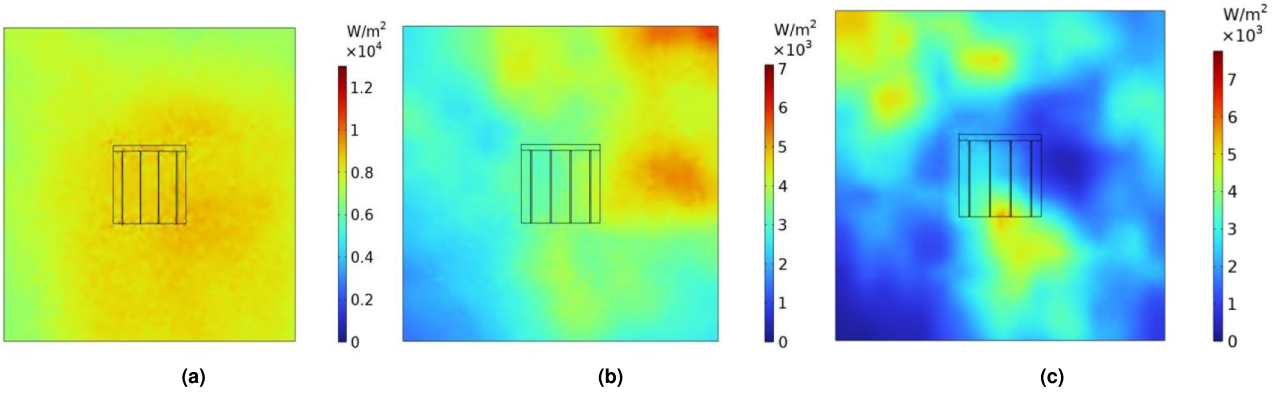

Fig. 8. Laser irradiation intensity distribution on the surface of PV-TEG receiver under different atmospheric turbulence structure constants.

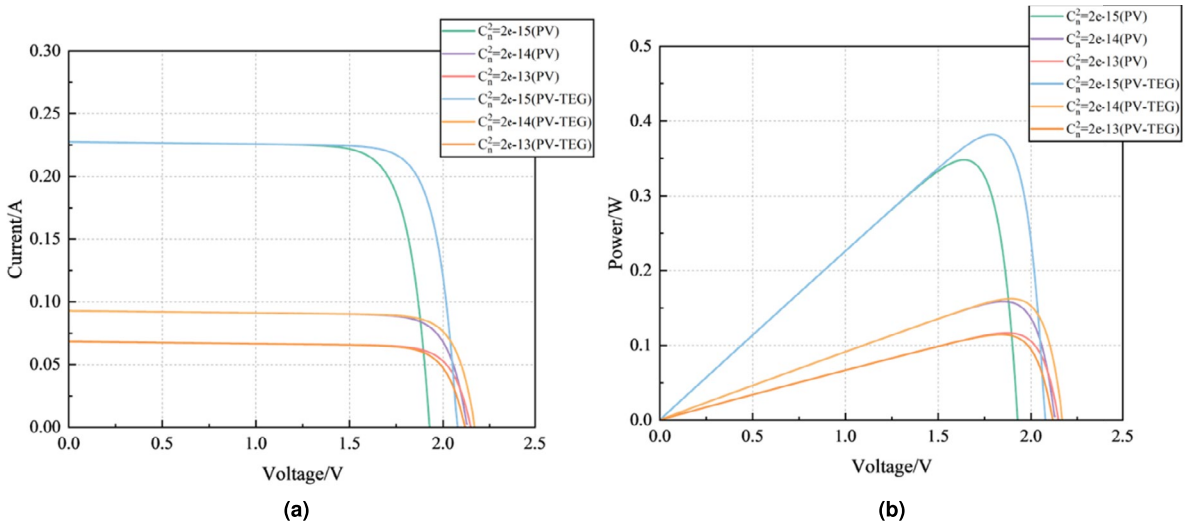

Fig. 9. I–V and P–V curves of the two receivers at different atmospheric turbulence intensities.

Laser power (W)	PV-TEG average irradiation intensity (W/m^2)	PV average irradiation intensity (W/m^2)	Maximum irradiation intensity (W/m^2)
2	1080.8	2949.7	4419.59
3	1621.2	4424.6	6629.39
4	2161.7	5899.4	8839.19
5	2702.1	7374.3	11408.99
6	3242.5	8849.2	13258.79

Table 9. Laser irradiation intensity on the surface of the combined PV-TEG receiver.

In summary, the PV-TEG receiver demonstrates a noticeable improvement in performance under the influence of atmospheric transmission. Although atmospheric uncertainties may result in a higher proportion of laser energy being utilized for the relatively low-efficiency thermoelectric conversion, the overall output power of the PV-TEG receiver consistently exceeds that of the standalone PV receiver. This superior performance can be attributed to the dual functionality of the PV-TEG receiver: the cooling effect on the photovoltaic components, which mitigates temperature-induced efficiency degradation, and the recovery of otherwise unused laser energy through thermoelectric conversion. These factors collectively enhance the overall energy utilization efficiency of the system, making the PV-TEG receiver a robust solution for wireless power transmission applications.

The influence of emitted laser power

In practical application scenarios, due to the influence of atmospheric transmission, the laser spot usually cannot completely cover the photovoltaic cells at the receiving end, resulting in a decrease in energy utilization. In order to increase the output power of LWPT, we preferentially use laser emitters with higher power. To explore the influence of laser irradiation intensity on the output characteristics of the PV-TEG system, the output characteristics of the PV-TEG receiver are simulated by changing the laser power. In multiphysics simulation, the Gaussian beam is used as the laser light source, and the laser irradiation intensity on the surface of the receiving end is calculated by ray tracing. The specific parameter settings of the Gaussian beam are the same as in Table 5, and only the power is changed. At the same time, in order to avoid the impact of spot offset, the geometry of the receiving end is set.The center is located in the same straight line as the laser light source. The laser radiation intensity parameters on the surface of the receiving end are listed in Table 9.

From the data presented in Table 9, it is evident that the laser irradiation intensity on the surface of the PV cell is significantly higher than that on the hot end of the TEG module. When the PV-TEG system is used as the receiving end, the laser spot exhibits a Gaussian distribution due to the divergence angle of the Gaussian beam. This results in a strong irradiation intensity at the center of the beam and weaker irradiation towards the periphery. Consequently, the GaAs photovoltaic cell, positioned at the center of the receiving end, receives higher laser irradiation intensity, enabling efficient conversion of energy into electrical power through the photoelectric effect.

The remaining fraction of the laser energy, which is not converted into electrical power by the PV cell, is absorbed as heat by the TEG module. This absorbed thermal energy generates a thermoelectric electromotive force due to the Seebeck effect. Given that the photoelectric conversion efficiency of GaAs photovoltaic cells can exceed 40%, whereas the thermoelectric conversion efficiency of TEG modules typically remains below 5%, it becomes evident that the central placement of the GaAs cells within the PV-TEG receiver structure is optimal.

This configuration ensures the maximization of laser energy utilization by prioritizing photoelectric conversion while also recovering residual energy through thermoelectric generation. Such a design not only enhances the overall energy output but also improves the thermal management of the system, contributing to its operational stability and efficiency.

Under varying laser power conditions, the non-uniform laser irradiation intensity on the surface of the photovoltaic cells and the TEG module leads to distinct temperature distributions. The temperature field is a critical factor influencing the overall output performance of the PV-TEG joint receiver, as it not only impacts the photoelectric performance of GaAs PV cells but also governs the thermoelectric conversion efficiency of the TEG module.

Figure 10a, b illustrate the overall temperature distribution of the PV-TEG joint receiver and the surface temperature distribution of the GaAs photovoltaic cells, respectively, under different laser power irradiation. As observed, with an increase in laser power, the temperature at both the cold and hot ends of the PV-TEG system, including the GaAs PV cell surface, increases progressively. This temperature rise is attributed to the greater absorption of laser energy, particularly at higher irradiation intensities.

It is evident that the GaAs PV cell, located at the geometric center of the PV-TEG receiver, experiences higher laser irradiation intensity due to the Gaussian beam profile. Consequently, the average surface temperature of the GaAs PV cell is marginally higher than the temperature of the surrounding hot end of the TEG module. This is because the central region, receiving the peak irradiation, accumulates more energy compared to the peripheral areas. Despite this localized temperature rise, the presence of the TEG module ensures an overall reduction in temperature through heat dissipation, enhancing the thermal management capabilities of the system. Therefore, the integration of the TEG module in the PV-TEG receiver effectively moderates the temperature distribution while leveraging the residual thermal energy for thermoelectric conversion. This dual function enhances the operational stability of the GaAs PV cells and contributes to improved overall system performance under increasing laser power conditions.

It can be observed from Fig. 11a that the temperature of the PV receiving terminal rises significantly with increasing laser power, from 308.62 K at 2 W to 338.65 K at 6 W. In contrast, the temperature increase at the PV-TEG receiving terminal is relatively moderate, rising only from 298.66 K to 309.72 K. The temperature at the PV-TEG receiving terminal remains more than 20 K lower than that of the PV terminal across all power levels. This temperature reduction is attributed to the TEG module, where the hot end, made of alumina ceramics with excellent thermal conductivity, effectively conducts excess heat away from the photovoltaic cell. This heat transfer mechanism reduces thermal accumulation, thereby maintaining the temperature of the PV-TEG cells at a significantly lower level. The subplot Fig. 11b illustrates the photoelectric conversion efficiency (PCE) of the PV and PV-TEG receivers and the thermoelectric conversion efficiency (TCE) of the TEG module as a function of laser power. For the PV receiver, the PCE decreases gradually with increasing laser power, reaching 41.8% at 6 W. This decline is due to the thermal degradation of PV cell performance caused by rising operating temperatures. In contrast, the PCE of the PV-TEG receiver first increases and then stabilizes at approximately 48%, highlighting the effectiveness of thermal management provided by the TEG module. The stable operating temperature of the PV-TEG cells mitigates the negative effects of thermal degradation, allowing for sustained TCE. Simultaneously, the TCE of the TEG module increases steadily with laser power, as the temperature difference between the hot and cold ends of the TEG module grows. At higher laser power levels, more residual thermal energy is absorbed, leading to an improvement in thermoelectric conversion efficiency. Finally, the total output power of the PV and PV-TEG receivers under varying laser powers and analyzes the power improvement ratio is compared in Fig. 11c. The output power of the PV-TEG receiving terminal includes contributions from both the photovoltaic cells and the thermoelectric generator. As laser power increases, the output power of both receivers increases; however, the growth rate of the PV-TEG system is significantly higher. At 2 W laser power, the output power of both systems is nearly identical. However,when the laser power is 6W, the output power of the PV-TEG receiver is 87.18W higher than that of the PV receiver. The yellow dashed line in the figure represents the output power

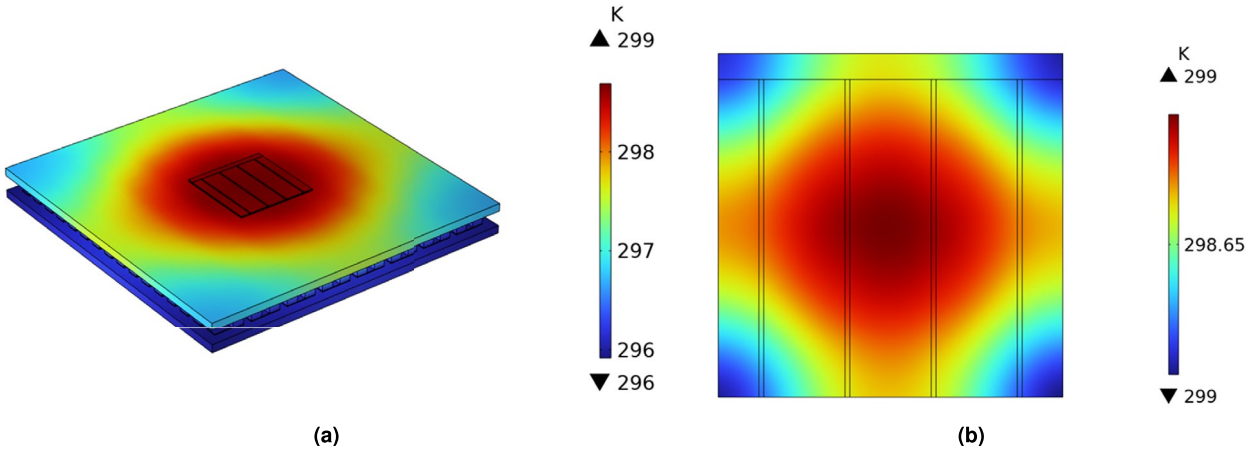

Fig. 10. Surface temperature distribution of: (**a**) PV-TEG joint receiver at P = 2W, (**b**) GaAs PV cells at P = 2W.

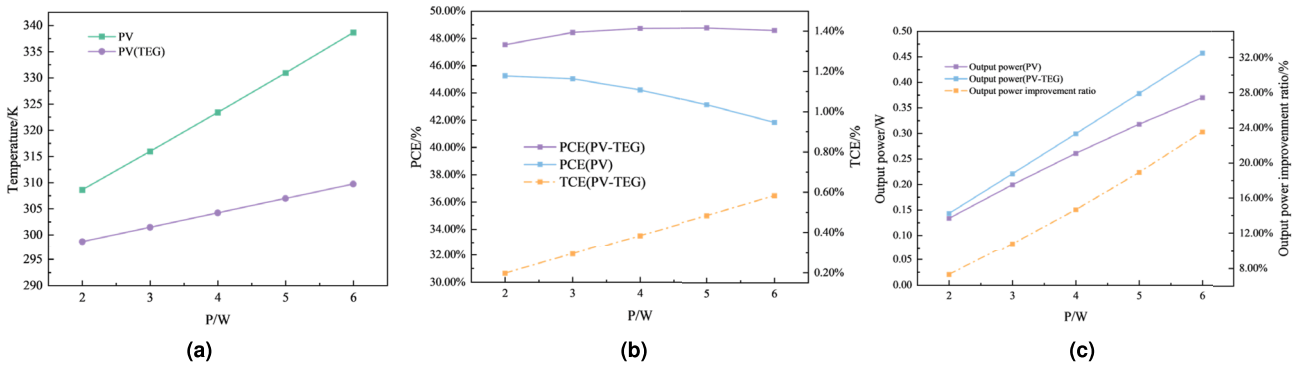

Fig. 11. (**a**) The temperature of photovoltaic cells at different receiving ends changes with power, (**b**) PV-TEG receiver conversion efficiency changes with power, (**c**) the output power and improvement of the receiving end change with the laser power.

improvement ratio of the PV-TEG system relative to the PV system, which exhibits a linear increase with rising laser power. This trend underscores the dual contribution of the PV-TEG system: the cooling effect provided by the TEG module enhances the PV cell efficiency, and the thermoelectric module generates additional power from the residual heat energy.

In summary, the PV-TEG receiver offers superior performance compared to the standalone PV receiver. The integration of the TEG module effectively reduces the operating temperature of the photovoltaic cells, stabilizes the photoelectric conversion efficiency, and contributes to an increase in overall system output power. The results highlight the significant advantages of the PV-TEG system in high-power laser wireless power transmission applications.

Conclusions

This paper comprehensively analyzee the output characteristics of the PV-TEG receiving terminal. The study evaluated the performance improvements of the PV-TEG system compared to the standalone PV receiver, including the medium-temperature difference power generation module. Both numerical simulations and experimental methods were employed to verify the output characteristics under identical conditions and atmospheric transmission effects. The key conclusions are as follows:

1. Thermal and electrical performance improvement:

The PV-TEG receiving terminal not only recovers unused laser energy-both energy exceeding the absorption range of the PV cell and that unconverted into electrical energy-but also plays a significant cooling role for the PV cells. Multiphysics simulations under identical light source conditions reveal that, at a laser power of 6 W, the operating temperature of the PV cells in the PV-TEG receiving terminal is reduced by 31.94 K compared to the PV-only receiver. This reduction in operating temperature results in an increase in the open-circuit voltage and maximum power output of the PV-TEG receiver. Specifically, the maximum power output is enhanced by 18.1% compared to the PV receiver. Additionally, the TEG module contributes an extra 27.28 mW of output power, leading to an overall improvement of 25.81% in the total output performance of the PV-TEG receiver relative to the PV-only system. In the future work, some verification of cooling methods such as water cooling will be carried out to ensure the integrity and rigor of the project.

2. Influence of laser power:

The effect of laser power on the output characteristics of the PV-TEG receiving terminal is investigated. Results indicate that as laser power increases, the photoelectric conversion efficiency (PCE) of the PV-TEG receiver initially rises and then stabilizes at values exceeding 48%. In contrast, the PCE of the standalone PV receiver decreases progressively with increasing laser power due to thermal degradation. Additionally, the thermoelectric conversion efficiency (TCE) of the TEG module increases steadily with higher laser power as the temperature gradient across the module intensifies. Overall, the PV-TEG receiving terminal demonstrates a more pronounced improvement in output power, further highlighting the effectiveness of integrating thermoelectric generation with photovoltaic cells.

In conclusion, the PV-TEG receiving terminal offers a substantial performance advantage over standalone PV systems. The integrated cooling effect and thermoelectric recovery significantly enhance energy conversion efficiency and overall output power, making the PV-TEG system a promising solution for laser wireless energy transmission applications.

Data availability

Regarding the article titled "Enhanced Laser Wireless Power Transmission Efficiency with a Novel PV-TEG Hybrid Receiver: Dual Thermal Management and Energy Recovery" submitted to Scientific Reports, the datasets used and/or analyzed during the current study are not publicly available but can be shared upon reasonable request to the corresponding author. Thank you!

Received: 25 January 2025; Accepted: 30 July 2025
Published online: 13 October 2025

References

1. Tesla, N. The transmission of electric energy without wires. In *Thirteenth Anniversary Number of the Electrical World & Engineer* (1904).
2. Liu, Z. et al. Advancements and challenges in wireless power transfer: A comprehensive review. *Nexus* **1**, 100014 (2024).
3. Özüpak, Y. Analysis and experimental verification of efficiency parameters affecting inductively coupled wireless power transfer systems. *Heliyon* **10**, e27420 (2024).
4. Kong, S., Bae, et al. An investigation of electromagnetic radiated emission and interference from multi-coil wireless power transfer systems using resonant magnetic field coupling. *IEEE Trans. Microwave Theory Tech.* **63**, 833–846 (2015).
5. Biao, H. et al. The x-band medium distance microwave wireless power transmission system based on multiplayer rectifier diode. *Energy Rep.* **9**, 367–373 (2023).
6. Wang, C. et al. The realization of the simultaneous wireless information and power transfer with the laser energy transform. *Meas. Sens.* **33**, 101197 (2024).
7. Zhang, Q. et al. Distributed laser charging: A wireless power transfer approach. *IEEE Internet Things J.* **5**, 3853–3864 (2018).
8. Meng, X., Li, X., Kong, D., Mallick, T. K. & Liu, C. Enhanced heat transfer characteristics using dimples in the receiving end of laser wireless power transmission system. *Appl. Therm. Eng.* **252**, 123619 (2024).
9. Meng, X., Li, X., Hou, Y., Zhang, P. & Liu, C. Comparative analysis of reverse truncated pyramid and other nonimaging concentrators as the receiver in laser wireless power transmission system. *nt. J. Energy Res.* **2024**, 5513198 (2024).
10. Ali, M., Behrooz, Z. M., Hadi, G. et al. Feasibility assessment of next-generation drones powering by laser-based wireless power transfer. *Opt. Laser Technol.* **143** (2021).
11. Brown, W. C. The history of wireless power transmission. *Solar Energy* **56**, 3–21 (1996).
12. Sprangle, P., Hafizi, B., Ting, A. et al. High-power lasers for directed-energy applications: Reply. *Appl. Opt.* (2017).
13. Modest, M. F. *Radiative Heat Transfer* (Academic Press, 2013).
14. Kyohoon, A. et al. Numerical simulation of high-energy laser propagation through the atmosphere and phase correction based on adaptive optics. *J. Korean Phys. Soc.* **79**, 918–929 (2021).
15. Meng, X., Liu, B., Lopez, C. F. A. & Liu, C. Multi-field coupling characteristics of photovoltaic cell under non-uniform laser beam irradiance. *Sustain. Energy Technol. Assess.* **52**, 101963 (2022).
16. Chong, K. et al. Dense-array concentrator photovoltaic prototype using non-imaging dish concentrator and an array of cross compound parabolic concentrators. *Appl. Energy* **204**, 898–911 (2017).
17. Shahpar, M., Hajinezhad, A. & Moosavian, F. S. The influence of diverse climate on the 3e analysis of energy, exergy, and environmental aspects of a hybrid module of thermoelectric generator and photovoltaic cells. *Results Eng.* **2**, 102337 (2024).
18. Parthiban, R., Ponnambalam, P. & Krishnamurthy, K. Analysis of area saving and efficiency enhancement of photovoltaic system combined with thermoelectric generator. *e-Prime-Adv. Electr. Eng. Electron. Energy* **8**, 100553 (2024).
19. Riyadi, B. W. T., Soumi, I. A., Haryanto, et al. Performance assessment of a photovoltaic cell coupled with a thermoelectric generator. *Eng. Proc.* **63**, 23 (2024).
20. Cao, F., Meng, X., Fang, H., Xu, Z. & Liu, C. Investigation of scaling criteria and matching method of overall cooling effectiveness with thermal radiation. *Appl. Therm. Eng.* **233**, 121063 (2023).
21. Pratap, A. S. et al. Experimental study of a novel photovoltaic-thermal-thermoelectric generator-based solar dryer for grapes drying. *Int. J. Green Energy* **21**, 1161–1173 (2024).
22. Meng, X., Liu, C. & Zhang, P. Optical model of thermal radiation loading system for turbine vane leading edge. *Energies* **14**, 8543 (2021).
23. Paul, I. On the isotropy of temperature fluctuations in passive scalar turbulence. *Phys. Fluids* **36** (2024).

Acknowledgements

This work was supported by the National Natural Science Foundation of China (No. 52176205), the National Natural Science Foundation of China (No. U2241268), and the Innovation Capacity Support Plan in Shaanxi Province of China (Grant No. 2023-CX-TD-19). IP acknowledges financial support from Khalifa University of Science and Technology, Abu Dhabi, UAE, via an internal funding grant FSU-2024-013/8474000720.

Author contributions

Professor Meng Xian-long was responsible for determining the theme of the article and the actual experimental research, Wang Zi-kun was responsible for the compilation of the article and some experimental work, Paul and Varghese were responsible for the editing and writing of the article, and Professor Liu Cun-liang was responsible for the communication work and the guidance of the article.

Declarations

Competing interests

The authors declare no competing interests.

Additional information

Correspondence and requests for materials should be addressed to L.C.-l.